Chemical Science

ROYAL SOCIETY OF CHEMISTRY

EDGE ARTICLE

View Article Online
View Journal | View Issue

Cite this: *Chem. Sci.*, 2024, **15**, 16752

All publication charges for this article have been paid for by the Royal Society of Chemistry

Received 7th May 2024
Accepted 12th September 2024

DOI: 10.1039/d4sc03006k

rsc.li/chemical-science

Does "zero-strain" lithiated spinel serve as a strain retardant and an irreversible phase transition regulator for layered oxide cathodes?†

Zixin Wu,[a] Qizheng Zheng,[a] Guiyang Gao,[b] Jianhua Yin,[a] Leiyu Chen,[a] Yonglin Tang,[a] Yawen Yan,[a] Huan Huang,*[c] Yaru Qin,*[d] Xiaoxiao Kuai,*[ae] Yu Qiao *[ae] and Shi-Gang Sun [ae]

Layered oxide cathodes encounter structural challenges during cycling, prompting the exploration of an ingenious heterostructure strategy, which incorporates stable components into the layered structure as strain regulators to enhance materials cycle stability. Despite considerable research efforts, identifying suitable, convenient, and cost-effective materials and methods remains elusive. Herein, focused on lithium cobalt oxide ($LiCoO_2$), we utilized its low-temperature polymorph as a strain-retardant embedded within a cathode. Our findings reveal that the low-temperature component, exhibiting zero-strain characteristic, adopts a complex configuration with a predominant lithiated spinel structure, also featuring both cubic-layered and typical-layered configurations. But this composite cathode exhibits a sluggish lithium-ion transport rate, attributed to Co&Li dislocation at the dual structural boundaries and the formation of cobalt(III) oxide. This investigation presents a pioneering endeavor in employing heterostructure strategies, underscoring the critical role of such strategies in component selection, which ultimately propels the advancement of layered oxide cathode candidates for Li-ion battery technology.

Introduction

The key to the superior capacity of layered oxide cathodes lies in continuous lithium (de)insertion within the oxide lattice framework, while the structural instability at high voltage has hindered their advancement.[1–4] For instance, our previous investigations[5] have demonstrated that lithium cobalt oxide ($LiCoO_2$, LCO) exhibits detrimental non-homogeneous delithiation beyond 4.6 V, characterized by the extreme depletion of lithium-ions within specific layers. This phenomenon induces significant lattice strain and an irreversible phase transition, ultimately leading to structural collapse and rapid capacity decay. The modification to enhance structural stability and uphold excellent cycle performance of layered oxide cathodes has been a topic of intensive research.[6–8] Nonetheless, conventional approaches, such as doping[9] and coating,[10] often introduce electrochemically inactive substances and reduce the initial capacity. Moreover, they generally fall short in adequately mitigating the challenges of lattice strain, which serves as the fundamental cause of structural failure. In this case, a pioneering heterostructure strategy[11,12] is proposed in order to realize the synergistic effect of different structures within the materials to improve the performance.

Despite much effort within the research community, identifying materials that match with the layered structure remains a formidable challenge. Recently, Jun Lu[13] and colleagues embedded a stable perovskite structure as a strain regulator into a layered oxide cathode. Additionally, investigations[14,15] have demonstrated that the incorporation of a small proportion of a spinel component into layered materials can enhance structural stability and extend the cycle life of the cathode. Therefore, we seek a cost-effective, purer and more streamlined method, which achieves greater coherent growth between polymorphs sharing the same elemental composition as layered materials. The good news is that a promising material, lithiated spinel LCO, originally identified as a polymorph of layered LCO in 1991,[16] has regained attention and further investigation led

[a]State Key Laboratory of Physical Chemistry of Solid Surfaces, Collaborative Innovation Center of Chemistry for Energy Materials (iChEM), Department of Chemistry, College of Chemistry and Chemical Engineering, Xiamen University, Xiamen, 361005, PR China. E-mail: kuaixiaoxiao@xmu.edu.cn; yuqiao@xmu.edu.cn
[b]State Key Laboratory of Physical Chemistry of Solid Surface, Fujian Key Laboratory of Surface and Interface Engineering for High Performance Materials, College of Materials, Xiamen University, Xiamen 361005, PR China
[c]The Institute of High Energy Physics, Chinese Academy of Sciences, Beijing 100190, PR China. E-mail: huanhuang@ihep.ac.cn
[d]School of Chemistry and Chemical Engineering, Qinghai Minzu University, Xining 810007, PR China. E-mail: szdxqyr@126.com
[e]Fujian Science & Technology Innovation Laboratory for Energy Materials of China (Tan Kah Kee Innovation Laboratory), Xiamen 361005, PR China

† Electronic supplementary information (ESI) available. See DOI: https://doi.org/10.1039/d4sc03006k

by the Thackeray group in recent years.[17] On the basis of this knowledge, we propose a strategy that embeds the spinel polymorph into the layered LCO, for three reasons. (1) The spinel LCO, reported as a zero-strain[18–20] material due to hard phase transitions during (dis)charge, may contribute to stabilizing the structure in dual-component materials. (2) The average voltage of 3.7 V in spinel LCO aligns with the operating voltage range of layered LCO, presenting an improvement over the conventional approach of doping electrochemically inactive substances. (3) The synthesis of the layered-spinel LCO requires a straightforward temperature adjustment, as the LCO prepared at low temperature adopts a spinel structure while a layered structure at high temperature.[21] However, the practice performance of the abovementioned material remains to be fully elucidated, needing further research and comprehensive characterization.

In this study, utilizing the classic layered oxide cathode, LCO, as an example, we successfully synthesized layered-spinel LCO and conducted a detailed investigation into its properties and mechanisms. This research addressed two key questions: Is the layered-spinel configuration a universally effective method for retarding strain and regulating irreversible phase transitions in layered oxide cathodes? What are the key points for continued optimization of this strategy? Our findings make a contribution to advancing the field of modifying layered-related heterostructure cathodes, ultimately enhancing the performance and dependability of lithium-ion secondary batteries.

Results and discussion

LCO has two polymorphs, which are determined by the synthetic temperature. The more commonly known layered LCO, commonly referred to as HT-LCO, is prepared at temperature exceeding 800 °C. In contrast, the lithiated spinel analogue, known as LT-LCO, is synthesized at a lower temperature of 400 °C.[22] However, in this study, we opt to refer to these polymorphs as layered LCO and (lithiated) spinel LCO, respectively, in order to underscore their unique structural characteristics. Fig. 1a shows the refined synchrotron radiation X-ray diffraction (XRD) patterns and structures of the layered LCO and lithiated spinel LCO. It is well known that layered $\{Li\}_{(3a)}[Co]_{(3b)}O_2$ (space group $R\bar{3}m$) has a distorted cubic-close-packed (ccp) oxygen array, which is reflected by the splitting of the (006)/(012) and (018)/(110) reflections (Fig. 1b).[23] In contrast, the lithiated spinel $\{Li_2\}_{(16c)}[Co_2]_{(16d)}O_4$ (space group $Fd\bar{3}m$) ideally does not exhibit such splitting. Nevertheless, as illustrated at

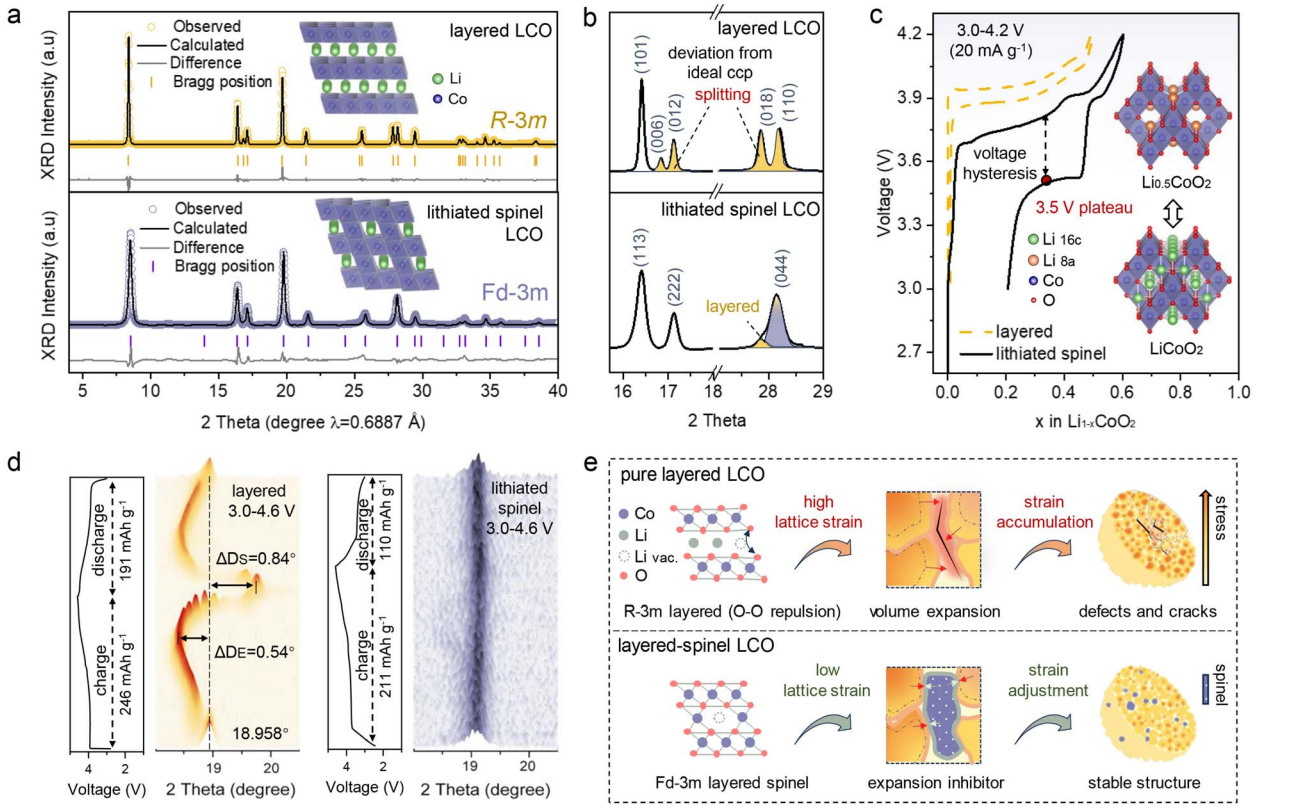

Fig. 1 (a) Refined synchrotron radiation XRD patterns of the pristine layered LCO and lithiated spinel LCO. Corresponding schematic illustrations of structures are shown in the inset. (b) Selected 2θ regions and component analysis. (c) Typical galvanostatic charge–discharge profiles curves of layered LCO and lithiated spinel LCO at a current density of 0.1C (1C = 200 mA g^{-1}) for 3–4.2 V (*vs.* Li/Li^+). The inset depicts a schematic diagram of the reversible phase transition between $Li_{0.5}CoO_2$ and $LiCoO_2$ within the spinel structure. (d) Main peaks of the *in situ* XRD patterns for layered LCO (left) and lithiated spinel LCO (right), along with the galvanostatic charge–discharge curve from 3 to 4.6 V (*vs.* Li/Li^+). The peak shift is denoted as ΔD_E when the *d*-spacing reaches its maximum expansion and as ΔD_s when the *d*-spacing reaches its minimum shrinkage. (e) The design principle of the layered-spinel heterostructure modification strategies for LCO.

the bottom of Fig. 1b, the broadening of the (044) peak suggests a minor presence of the layered LCO. The detailed quantification presented in Table S2† indicates a negligible proportion of this layered phase, leading us to disregard its influence in the subsequent analysis.

Fig. 1c displays the initial open circuit voltage (OCV) profiles of lithium cells containing layered LCO and lithiated spinel LCO cathodes, which cycle between 3 and 4.2 V. The OCV profile for Li/LT-LCO exhibits charging and discharging plateaus at 3.7 V and 3.5 V, respectively, which correspond to the well-known two-phase reaction between stoichiometric spinel $\{Li_{0.5}\}_{(8a)}[Co]_{(16d)}O_2$ and lithiated spinel $\{Li\}_{(16c)}[Co]_{(16d)}O_2$ structures. Moreover, the plateaus at approximately 3.9 V align with the electrochemical behavior characteristic of the layered LCO, which is consistent with our previous XRD results. Notably, we observe an evident voltage hysteresis for the lithiated spinel LCO component but not for the layered LCO, suggesting that the path followed during de-lithiation differs from that taken on lithiation. It is conceivable that the observed phenomenon correlates with structural modifications, and a more in-depth analysis will be presented in subsequent sections.

The main peaks in the *in situ* XRD results obtained during the initial charge and discharge for Li/layered LCO and Li/spinel LCO half-cells are shown in Fig. 1d. Obviously, the main peak of layered LCO undergoes a complex shifting and splitting process, which means that the LCO cathode has a drastic change in *d*-spacing, phase structure and volume.[24,25] In striking contrast, *in situ* XRD of spinel LCO does not provide any significant evidence of a peak shift during the initial charge–discharge process (Fig. S3†). The change to the unit cell volume approaches zero, aligning with the characteristics of zero-strain materials. As widely recognized, the delithiation process typically leads to an increase in the *d*-spacing of layered LCO due to the O–O repulsion,[26] resulting in lattice strain and subsequent volume expansion in localized regions (Fig. 1e). This strain accumulation often correlates with the formation of defects and cracks.[27–29] Consequently, we hypothesize that integrating the zero-strain lithiated spinel structure into the layered LCO, herein referred to as layered-spinel LCO, may offer potential advantages in mitigating strain-induced effects and suppressing irreversible phase transitions. This strategic integration could serve to diminish the occurrence of strain-related defects and cracks.

The synthesis of layered-spinel LCO was achieved through careful manipulation of the synthesis temperature and duration, as detailed in the experimental procedures outlined in the ESI.† Fig. 2a presents the synchrotron XRD patterns of the

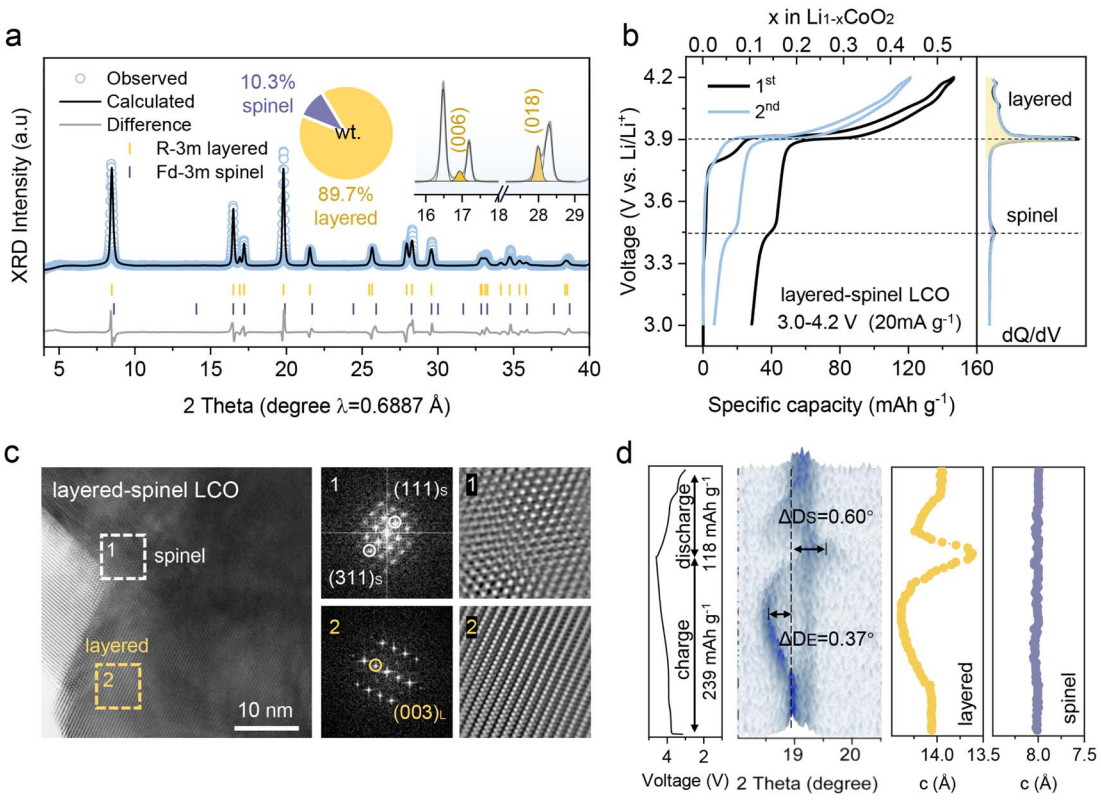

Fig. 2 (a) Refined synchrotron radiation XRD pattern of the pristine layered-spinel LCO. The inset displays selected 2θ regions and component analysis. (b) Charge–discharge profiles and the corresponding d*Q*/d*V* chart during discharge of the layered-spinel LCO at a current density of 0.1C for 3–4.2 V (*vs.* Li/Li^+). (c) HR-TEM image of the layered-spinel LCO. The FFT and IFFT images obtained from the corresponding regions of the cathode are displayed on the right side. (d) Main peaks of the *in situ* XRD patterns for the layered-spinel LCO and galvanostatic charge–discharge curve from 3 to 4.6 V (*vs.* Li/Li^+). The c lattice parameters of the layered (yellow) and spinel (purple) phases, obtained from the refinement, are shown in the right panel.

layered-spinel LCO, and our refined analysis revealed a lithiated spinel component comprising approximately 10.3% of the overall composition. The inset presents distinct signals corresponding to the (006) and (018) peaks of layered LCO. Furthermore, the voltage profile exhibited clear plateaus corresponding to both the layered and lithiated spinel components, as depicted by the dQ/dV peaks at ~3.9 V and 3.45 V during the discharge process in the right panel of Fig. 2b. High-resolution transmission electron microscopy (HR-TEM) images and fast Fourier transforms (FFTs) of the layered-spinel LCO sample reveal distinct localized regions corresponding to the spinel (region 1) and layered (region 2) configurations within individual grains (Fig. 2c). To delve deeper into the structural characteristics, *in situ* XRD analysis was conducted, as depicted in Fig. 2d. The XRD patterns exhibit two sets of evolving peaks, aligning with the expected variations in the primary peaks of the layered and spinel LCO phases as previously discussed, which are further supported by changes in the unit cell parameter c. It is worth emphasizing that the layered phase of the composite cathode exhibits reduced interlayer expansion and shrinkage (smaller ΔD_E and ΔD_s) compared to the pure layered LCO (Fig. 1d). This indicates that the spinel component functions as a strain retardant and an irreversible phase transition regulator. Moreover, given the minimal difference in charging capacity between the two batteries, this effect is deemed negligible. In summary, we have synthesized a layered-spinel LCO material that appears to exhibit structural characteristics consistent with our initial expectations. However, it is essential to critically evaluate whether this material truly meets the expected electrochemical properties and effects. To address this question and elucidate any unsatisfactory aspects of this material, the following discussion provides an in-depth analysis.

Fig. 3 illustrates the electrochemical profiles of both layered LCO and layered-spinel LCO. Regrettably, the layered-spinel LCO exhibits a diminished initial capacity and accelerated capacity decay in comparison to the layered LCO when cycling between 3 and 4.2 V (Fig. 3a and b). We want to optimize its performance by adjusting the experimental parameters and conditions, such as the proportion of the two components. To further explore, we synthesized two additional materials with spinel ratios exceeding 10% (600 °C 1 h-LCO, Fig. 3c) and falling below 10% (700 °C 1 h-LCO, Fig. 3d) by adjusting the synthesis temperature and duration, yet their performance remained unsatisfactory. Moreover, an increase in voltage to 4.6 V was implemented, still yielding poor performance for the layered-spinel LCO (Fig. 3e and f). As the cycling proceeds, a noticeable trend emerges wherein the voltage of charging plateaus (~3.7 V) exhibits an increase, while that of discharging plateaus (~3.5 V) undergoes a decrease. This observation suggests an elevated overpotential requisite for lithium-ion (de)intercalation, potentially linked to structural degradation of the spinel component. This phenomenon is further supported by the decreasing duration of the plateaus. Additional electrochemical data obtained under diverse conditions are provided in Fig. S5–S8.† Overall, the performance of the layered-spinel LCO falls short of expectations, indicating that the inclusion of spinel components does not lead to performance enhancements. Why

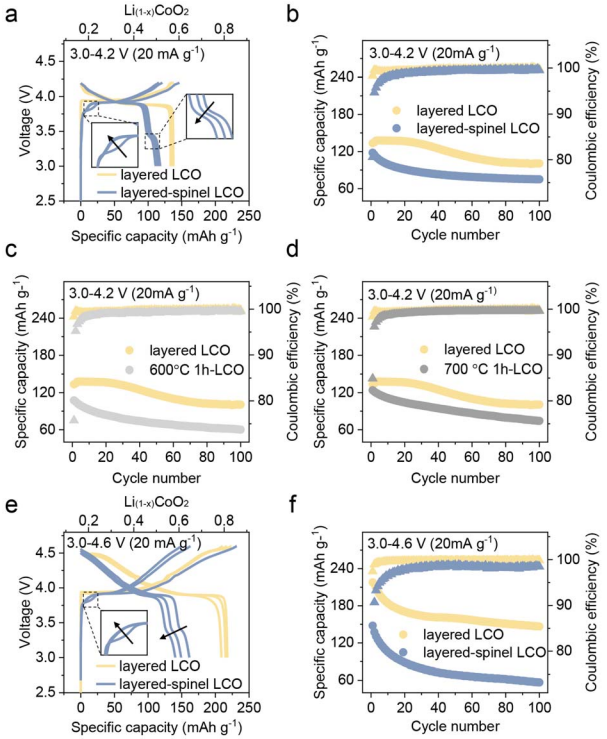

Fig. 3 Electrochemical performance of different LCO batteries. (a and e) Charge–discharge profiles of layered LCO and layered-spinel LCO at 0.1C, in a voltage range of (a) 3–4.2 V and (e) 3–4.6 V (*vs.* Li/Li$^+$). (b–d) Cycle performance of different cell configurations: (b) layered-spinel LCO, (c) 600 °C 1 h- LCO (spinel ratio > 10%), and (d) 700 °C 1 h-LCO (spinel ratio < 10%), compared to the layered LCO at a current density of 0.1C for 3–4.2 V (*vs.* Li/Li$^+$). (f) Cycle performance comparison of the layered-spinel LCO and the layered LCO at 0.1C for 3–4.6 V (*vs.* Li/Li$^+$).

do these results contradict our initial hypotheses? Could it be that our understanding of the distinct characteristics of the various LCO structures is incomplete? In order to elucidate the underlying reasons for these findings, we delve into a detailed structural analysis of the material.

Fig. 4a–c present the Co K-edge X-ray absorption near edge structure (XANES) data for layered LCO, layered-spinel LCO and spinel LCO at various states. The observed resonance at 7710 eV is ascribed to the 1s to 3d transition of Co orbitals, with its intensity likely stemming from pure electric quadrupole coupling and/or hybridization of d and dipole-allowed p orbitals.[30,31] Therefore, the presence and intensity of this peak indicate that the CoO_6 octahedra are distorted. Additionally, the feature at 7720 eV is associated with an electric-dipole-allowed 1s to 4p transition followed by O to Co charge transfer (ligand-to-metal charge transfer, LMCT). The gradual disappearance of this feature is linked to the increased distortion of the CoO_6 octahedra, resulting in reduced overlap between the O 2p and Co orbitals. Furthermore, the observed shift of the Co absorption edge towards higher energy is consistent with the oxidation of Co^{3+}.[32] Additional discussion on charge compensation is provided in Fig. S9,† while this aspect is not a key factor in this study. In summary, the CoO_6 octahedra of these

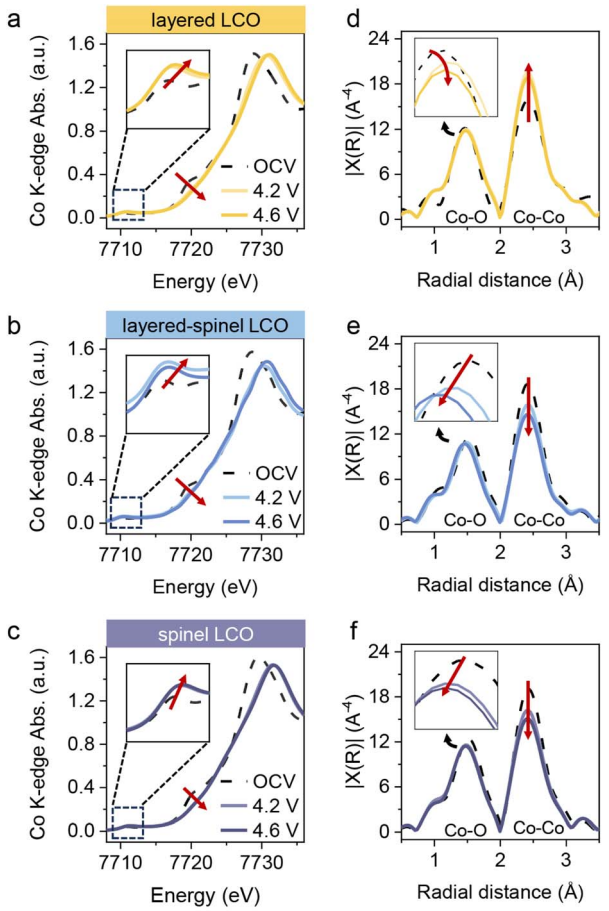

Fig. 4 (a–c) Normalized *ex situ* Co K-edge XANES spectra at states of pristine, 4.2 V and 4.6 V (*vs.* Li/Li$^+$) for (a) layered LCO, (b) layered-spinel LCO and (c) spinel LCO. (d–f) Co K-edge EXAFS spectra at states of pristine, 4.2 V and 4.6 V (*vs.* Li/Li$^+$) for (d) layered LCO, (e) layered-spinel LCO and (f) spinel LCO.

three materials are distorted during the charging process. However, as the XANES data show minimal variance, emphasis is placed on the utilization of EXAFS spectra to obtain more detailed structural information. Fig. 4d exhibits the corresponding Co K-edge extended X-ray absorption fine structure (EXAFS) data for layered LCO, illustrating first shell Co–O and second shell Co–Co scattering events at distances of 1.4 and 2.4 Å, respectively.[33] The Co–O interactions exhibit a noticeable shift towards higher distances followed by a subsequent shift towards lower distances, accompanied by a decrease in intensity during the charging process. This behavior indicates fluctuations in the Co–O distance and a reduction in the coordination number, which is caused by the phase transition and distortion of the CoO_6 octahedron. Furthermore, the intensity of the Co–Co interactions increases at a fixed distance and aligns with the more perpendicularly compressed structure (O3 to O1) due to the gliding of slabs. In contrast, as depicted in Fig. 4e and f, the Co–O peaks observed in the other cathodes display a larger shift than that observed in layered LCO, suggesting more severe lattice shrinkage and generation of defects. Besides, the intensity of Co signals decreases both in the first and second coordination after charging, indicating a decrease in the degree of long-range order.[34] This phenomenon may be attributed to the formation of a disordered (rock salt) phase, which is consistent with our analysis of the electrochemical profiles. Overall, the inclusion of spinel LCO in cathode materials leads to more pronounced structural distortion compared to pure layered LCO, and this finding challenges the assumption that such a spinel component enhances stability and structural improvements. Consequently, revisiting the investigation of lithium spinel LCO itself can provide insights into the underlying reasons for the subpar performance of layered-spinel LCO.

In the preceding section, we denoted LT-LCO as spinel LCO to underscore its structural characteristics. Nonetheless, upon scrutinizing the experimental results, uncertainties arise regarding the precise structural characteristics of LT-LCO. Previous investigation[35] by Gummow *et al.* suggested that the LT-LCO exhibits a perfect ccp layered structure (hereinafter termed "cubic-layered" LCO) with a minor percentage of the lithium and cobalt ions mixing in the other layers. To validate the structural information, neutron powder diffraction (NPD) analyses were conducted on the LT-LCO sample (Fig. 5a and b). Consistent with the XRD findings, the LT-LCO spectra exhibited not only the predominant phase but also revealed the presence of a minor proportion of layered components. Notably, owing to the heightened sensitivity of NPD towards lighter elements such as lithium and oxygen compared to XRD, signals corresponding to lithium carbonate (Li_2CO_3) were discerned in the NPD data, originating from residual reactions.[36]

Confusingly, the NPD assessment presented a quandary in determining the primary phase, as both spinel (Fig. 5a) and cubic-layered structures (Fig. 5b) exhibited compatibility with the experimental results, which are also in agreement with the refined results from XRD (Fig. S1†). The distinction between the cubic-layered LCO and the spinel LCO proved to be challenging, underscoring the intricate nature of the LCO material synthesized at 400 °C as a composite multiphase entity encompassing spinel, cubic-layered, and layered structures, alongside unreacted Li_2CO_3. Nevertheless, the unique electrochemical performance exhibited by this material diverges from that of the conventional HT-LCO, suggesting a predominant spinel structure. As illustrated in Fig. 5c, HR-TEM coupled with corresponding FFT/IFFT analyses unveiled the presence of spinel and cubic-layered regions within the pristine LT-LCO configuration, which is consistent with the above conclusion. Subsequent to the initial cycle, discernible degradation of the LT-LCO surface was observed, manifesting as spinel Co_3O_4 formation[37,38] alongside regions exhibiting an amorphous character.

Upon restudy, it has become evident that the structural composition of LT-LCO is notably intricate. This realization has prompted an investigation into the underlying reasons for its suboptimal performance, and our research focuses on the diffusion of lithium-ions. Analysis of diffusion coefficients using the galvanostatic intermittent titration technique (GITT) reveals sluggish lithium-ion diffusion within the LT-LCO framework (Fig. S10†). Drawing from these observations, we provide an explanation of the failure mechanism that underlies

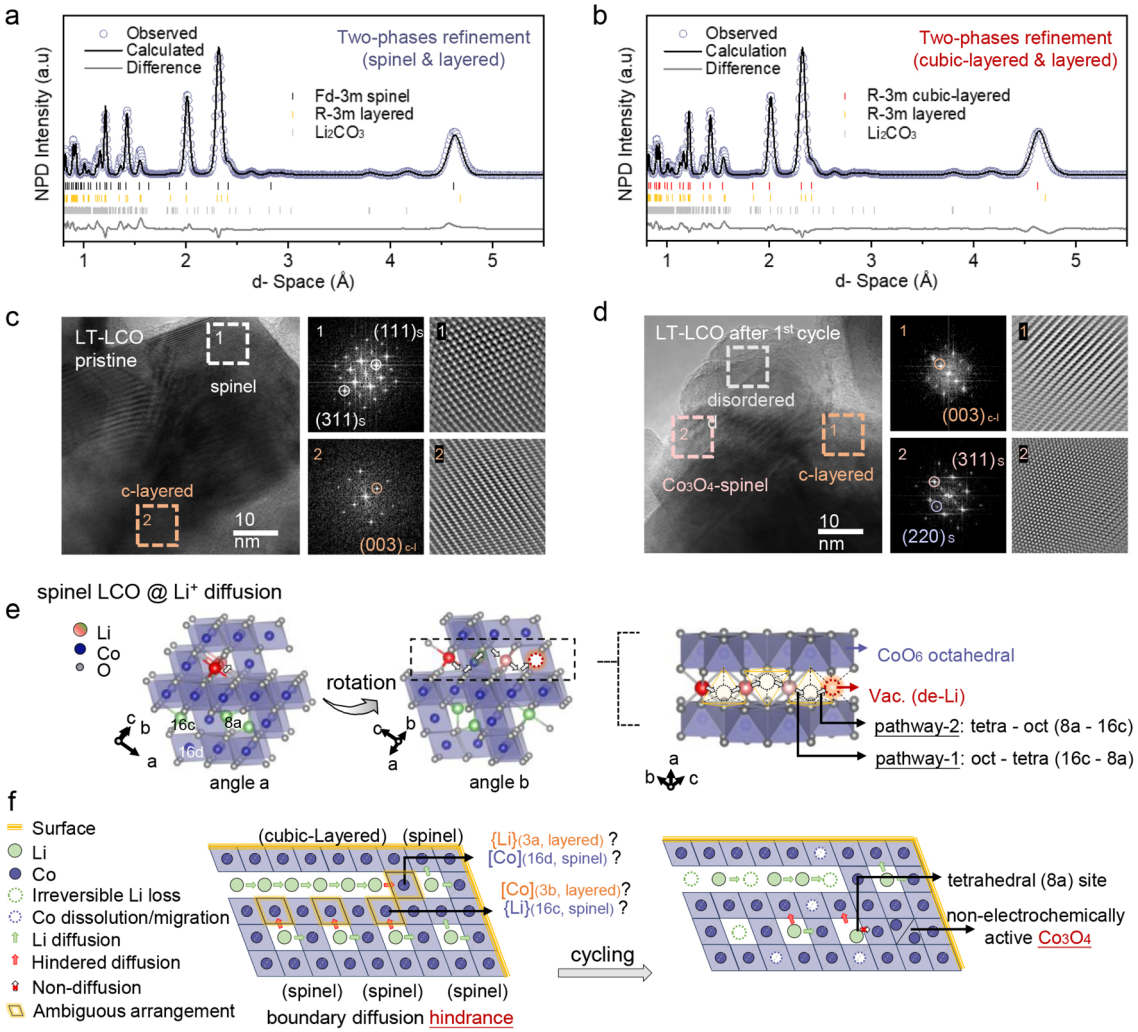

Fig. 5 (a and b) Refined NPD pattern of pristine LT-LCO with two different main phases: (a) spinel and (b) cubic-layered. (c and d) HR-TEM images and corresponding FFT/IFFT images of (c) pristine LT-LCO and (d) LT-LCO after the 1st cycle. (e) A schematic illustration of the lithium diffusion pathway within the spinel structure. (f) A schematic illustration of lithium diffusion and deterioration analysis for LT-LCO.

the performance of LT-LCO. The left panel in Fig. 5e illustrates the lithium-ion diffusion pathway of the spinel structure from two distinct angles, providing valuable insight for subsequent analysis. It is noteworthy that there appears to be a hindrance to the lithium-ion diffusion pathway by cobalt ions when viewed from angle *b*, while in reality, it is merely a visual misunderstanding, as demonstrated by the unhindered lithium-ion diffusion channel from angle a. In the spinel LCO structure, cobalt ions occupy the 16d position while lithium resides in the 16c position. During the delithiation process, lithium-ions initially transition to the 8a position before migrating to an adjacent vacant lithium site at 16c. For the cubic-layered structure, the lithium-ions are set at the 3a position, while the cobalt ions lie at the 3b position.

Following an analysis of lithium-ion diffusion pathways within the spinel structure, a deeper understanding of the diffusion mechanisms inherent in LT-LCO, concluding both spinel and cubic-layered structures, has been obtained. In the early stages of delithiation of LT-LCO, lithium-ions migrate towards the surface. Notably, at the boundary of these, the spatial arrangement of certain ions remains ambiguous: (1) for the diffusion path in the cubic-layered region, the boundary may exhibit an arrangement of $\{Li\}_{(3a)}$ or $[Co]_{(16d)}$; (2) for the diffusion path in the spinel region, the boundary may exhibit an arrangement of $\{Li\}_{(16c)}$ or $[Co]_{(3b)}$. In all events, the presence of cobalt ions poses a hindrance to the diffusion of lithium-ions, thereby impeding the rate of lithium-ion transport. Additionally, previous investigation[39] by Chu Zhang *et al.* revealed that the Li-depleted spinel $Li_{0.5}CoO_2$ ($LiCo_2O_4$), arising from the delithiated spinel LCO (Li_2CoO_4), demonstrates a heightened tendency to transition into cobalt(III) oxide (Co_3O_4) due to energetic considerations when compared to the Li-deficient layered LCO, which is consistent with the above HR-TEM results. After cycles, the formation of non-electrochemically active Co_3O_4 makes lithium-ion diffusion more difficult. Moreover, issues such as cobalt dissolution (migration)[40] and irreversible lithium loss lead to a progressive deterioration of the material structure.

Conclusions

In this study, we successfully synthesize layered-spinel composite LCO cathodes with a 10% lithiated spinel ratio by controlling calcination temperature and duration. Through comprehensive structural analyses, particularly employing *ex situ* XRD, NPD and HR-TEM, we made an unexpected discovery contrary to the prevailing understanding: the synthesis of a pure lithiated spinel phase in LCO is exceptionally challenging; instead, the low-temperature LCO (LT-LCO), actually exhibits a complex structure. It predominantly manifests a primary lithiated spinel structure while concurrently harboring cubic-layered and layered configurations. The good news is that we demonstrate that the LT-LCO exhibits zero-strain behavior, evidenced by minimal variation in diffraction peaks during (dis) charge processes, which renders it a promising strain retardant. The bad news is that the electrochemical performance of layered-spinel LCO with a heterostructure failed to meet the expectations. Moreover, Co K-edge EXAFS characterization unveiled its shortcomings of a relatively unstable structure, attributed to sluggish lithium ion transport kinetics in boundary regions and the lower energy level of structural degradation into Co_3O_4. In light of these findings, while the addition of spinel components alleviates strain and inhibits irreversible phase transitions within the layered phase, unanticipated hindered lithium-ion diffusion leads to unsatisfactory performance. It becomes evident that the layered-spinel heterostructure is not a fully applicable modification strategy for layered cathodes, highlighting the importance of component selection and design. To refine and advance this approach, we propose two promising avenues. First, incorporating an aluminum (Al) substitute in layered-spinel LCO could address the complex multiphase issues observed and facilitate smoother lithium-ion diffusion, as it has been shown to inhibit the formation of cubic-layer phases and stabilize spinel structures. Second, further exploration of heterostructure strategies involving nickel (Ni), manganese (Mn), and cobalt (Co)-containing materials is warranted. This work offers valuable insights and research directions for investigating this series of cathodes, ultimately advancing high-energy-density layered oxide cathodes with enhanced structural stability.

Data availability

The data that support the findings of this study are available within the article and its ESI.†

Author contributions

Z. W. and Y. Q. contributed to the design of the research and performed the experimental data analysis. Z. W. conducted the materials synthesis and electrochemistry and evaluated cell performance. Q. Z. conducted the HR-TEM experiments and related data analysis. Y. Y. conducted the soft-XAS experiments. Y. T. and L. C. conducted the hard-XAS experiments. J. Y., H. H. and X. K. conducted the analysis of the XAS results. G. G. conducted the XRD experiment. H. H., Y. Q., X. K. and Y. Q. supervised the work. All authors discussed the results and co-wrote and commented on the manuscript.

Conflicts of interest

The authors declare no competing financial interests.

Acknowledgements

This work was partially supported by the National Natural Science Foundation of China (grant no. 22179111, 22021001, 22109186, 52250402, 52025025 and 22288102), the Ministry of Science and Technology of China (grant no. 2021YFA1201900), the Basic Research Program of Tan Kah Kee Innovation Laboratory (grant no. RD2021070401), the Principal Fund from Xiamen University (grant no. 20720210015), Fundamental Research Funds for the Central Universities (grant no. 20720220010) and the Beijing Natural Science Foundation (grant no. Z190010). This research also employed the resources of the National Synchrotron Radiation Research Center (NSRRC) in Hsinchu, Taiwan, R.O.C. This research also employed the resources of the Shanghai Synchrotron Radiation Facility BL14B1, BL11B and B02 beamline station (SSRF, under Contract No. 2021-SSRF-PT-017208, 2022-SSRF-PT-019758, and 2022-SSRF-PT-021637), Hefei National Synchrotron Radiation Laboratory (NSRL-USTC, under Contract No. 2021-HLS-PT-004529, 2021-HLS-PT-004156, and 2021-HLS-PT-004241), Beijing Synchrotron Radiation Laboratory 1W1B, 4B9A and 4B9B beamlines station (under Contract No. 2021-BEPC-PT-005771, 2021-BEPC-PT-005765, 2021-BEPC-PT-005760, and 2022-BEPC-PT-006478), and China Spallation Neutron Source (CSNS, under contract no. P1621080200036 and P1621122000008).

Notes and references

1 Y. Lyu, X. Wu, K. Wang, Z. Feng, T. Cheng, Y. Liu, M. Wang, R. Chen, L. Xu, J. Zhou, Y. Lu and B. Guo, *Adv. Energy Mater.*, 2020, **11**, 2000982.
2 S. Liu, P. J. West, H. Zhong, J. Bai, E. Stavitski, D. Leshchev, A. C. Marschilok, E. S. Takeuchi, D. C. Bock and K. J. Takeuchi, *Chem. Mater.*, 2023, **35**, 8857–8871.
3 T. Liu, J. Liu, L. Li, L. Yu, J. Diao, T. Zhou, S. Li, A. Dai, W. Zhao, S. Xu, Y. Ren, L. Wang, T. Wu, R. Qi, Y. Xiao, J. Zheng, W. Cha, R. Harder, I. Robinson, J. Wen, J. Lu, F. Pan and K. Amine, *Nature*, 2022, **606**, 305–312.
4 X. Liu, G.-L. Xu, V. S. C. Kolluru, C. Zhao, Q. Li, X. Zhou, Y. Liu, L. Yin, Z. Zhuo, A. Daali, J.-J. Fan, W. Liu, Y. Ren, W. Xu, J. Deng, I. Hwang, D. Ren, X. Feng, C. Sun, L. Huang, T. Zhou, M. Du, Z. Chen, S.-G. Sun, M. K. Y. Chan, W. Yang, M. Ouyang and K. Amine, *Nat. Energy*, 2022, **7**, 808–817.
5 Z. Wu, G. Zeng, J. Yin, C.-L. Chiang, Q. Zhang, B. Zhang, J. Chen, Y. Yan, Y. Tang, H. Zhang, S. Zhou, Q. Wang, X. Kuai, Y.-G. Lin, L. Gu, Y. Qiao and S.-G. Sun, *ACS Energy Lett.*, 2023, **8**, 4806–4817.
6 X. Cao, Y. Qiao, M. Jia, P. He and H. Zhou, *Adv. Energy Mater.*, 2021, **12**, 2003972.

7 H. Yang, H. H. Wu, M. Ge, L. Li, Y. Yuan, Q. Yao, J. Chen, L. Xia, J. Zheng, Z. Chen, J. Duan, K. Kisslinger, X. C. Zeng, W. K. Lee, Q. Zhang and J. Lu, *Adv. Funct. Mater.*, 2019, **29**, 1808825.
8 S. Kalluri, M. Yoon, M. Jo, S. Park, S. Myeong, J. Kim, S. X. Dou, Z. Guo and J. Cho, *Adv. Energy Mater.*, 2016, **7**, 1601507.
9 Y. Wang, Z. Yang, Y. Qian, L. Gu and H. Zhou, *Adv. Mater.*, 2015, **27**, 3915–3920.
10 J. Zhang, H. Zhang, R. Gao, Z. Li, Z. Hu and X. Liu, *Phys. Chem. Chem. Phys.*, 2016, **18**, 13322–13331.
11 X. Zhu, F. Meng, Q. Zhang, L. Xue, H. Zhu, S. Lan, Q. Liu, J. Zhao, Y. Zhuang, Q. Guo, B. Liu, L. Gu, X. Lu, Y. Ren and H. Xia, *Nat. Sustain.*, 2020, **4**, 392–401.
12 S. Hu, Y. Li, Y. Chen, J. Peng, T. Zhou, W. K. Pang, C. Didier, V. K. Peterson, H. Wang, Q. Li and Z. Guo, *Adv. Energy Mater.*, 2019, **9**, 1901795.
13 L. Wang, T. Liu, T. Wu and J. Lu, *Nature*, 2022, **611**, 61–67.
14 E. Lee, J. Blauwkamp, F. C. Castro, J. Wu, V. P. Dravid, P. Yan, C. Wang, S. Kim, C. Wolverton, R. Benedek, F. Dogan, J. S. Park, J. R. Croy and M. M. Thackeray, *ACS Appl. Mater. Interfaces*, 2016, **8**, 27720–27729.
15 S. Park, S. Kang, C. Johnson, K. Amine and M. Thackeray, *Electrochem. Commun.*, 2007, **9**, 262–268.
16 R. J. Gummow, M. M. Thackeray, W. David and S. Hull, *Mater. Res. Bull.*, 1992, **27**, 327–337.
17 S. Kim, V. I. Hegde, Z. Yao, Z. Lu, M. Amsler, J. He, S. Hao, J. R. Croy, E. Lee, M. M. Thackeray and C. Wolverton, *ACS Appl. Mater. Interfaces*, 2018, **10**, 13479–13490.
18 K. Ariyoshi, Y. Orikasa, K. Kajikawa and Y. Yamada, *J. Mater. Chem. A*, 2019, **7**, 13641–13649.
19 W. Kong, J. Zhang, D. Wong, W. Yang, J. Yang, C. Schulz and X. Liu, *Angew. Chem., Int. Ed.*, 2021, **60**, 27102–27112.
20 E. Lee, B. J. Kwon, F. Dogan, Y. Ren, J. R. Croy and M. M. Thackeray, *ACS Appl. Energy Mater.*, 2019, **2**, 6170–6175.
21 E. Rossen, J. N. Reimers and J. R. Dahn, *Solid State Ionics*, 1993, **62**, 53–60.
22 K. Ariyoshi, K. Yuzawa and Y. Yamada, *J. Phys. Chem. C*, 2020, **124**, 8170–8177.
23 X. Lu, Y. Sun, Z. Jian, X. He, L. Gu, Y.-S. Hu, H. Li, Z. Wang, W. Chen, X. Duan, L. Chen, J. Maier, S. Tsukimoto and Y. Ikuhara, *Nano Lett.*, 2012, **12**, 6192–6197.
24 H. Ben Yahia, M. Shikano and H. Kobayashi, *Chem. Mater.*, 2013, **25**, 3687–3701.
25 Z. Chen, Z. Lu and J. R. Dahn, *J. Electrochem. Soc.*, 2002, **149**, A1604–A1609.
26 S. Li, Y. Sun, A. Gao, Q. Zhang, X. Lu and X. Lu, *Proc. Natl. Acad. Sci. U. S. A.*, 2022, **119**, e2120060119.
27 S. Yamakawa, N. Nagasako, H. Yamasaki, T. Koyama and R. Asahi, *Solid State Ionics*, 2018, **319**, 209–217.
28 J.-Y. Wang, S.-N. Guo, X. Wang, L. Gu and D. Su, *J. Electrochem.*, 2022, **28**, 2108431.
29 G. L. Xu, X. Liu, A. Daali, R. Amine, Z. Chen and K. Amine, *Adv. Funct. Mater.*, 2020, **30**, 2004748.
30 C. J. Patridge, C. T. Love, K. E. Swider-Lyons, M. E. Twigg and D. E. Ramaker, *J. Solid State Chem.*, 2013, **203**, 134–144.
31 W. S. Yoon, K. K. Lee and K. B. Kim, *J. Electrochem. Soc.*, 2000, **147**, 2023–2028.
32 M. Okubo and A. Yamada, *ACS Appl. Mater. Interfaces*, 2017, **9**, 36463–36472.
33 W. Kong, D. Zhou, Q. Zhang, D. Wong, K. An, C. Schulz, N. Zhang, J. Zhang and X. Liu, *Adv. Funct. Mater.*, 2022, **33**, 2211033.
34 B. Zhang, Y. Zhang, X. Wang, H. Liu, Y. Yan, S. Zhou, Y. Tang, G. Zeng, X. Wu, H. G. Liao, Y. Qiu, H. Huang, L. Zheng, J. Xu, W. Yin, Z. Huang, Y. Xiao, Q. Xie, D. L. Peng, C. Li, Y. Qiao and S. G. Sun, *J. Am. Chem. Soc.*, 2023, **145**, 8700–8713.
35 R. J. Gummow, D. C. Liles and M. M. Thackeray, *Mater. Res. Bull.*, 1993, **28**, 235–246.
36 Y. Yan, Q. Fang, X. Kuai, S. Zhou, J. Chen, H. Zhang, X. Wu, G. Zeng, Z. Wu, B. Zhang, Y. Tang, Q. Zheng, H. G. Liao, K. Dong, I. Manke, X. Wang, Y. Qiao and S. G. Sun, *Adv. Mater.*, 2023, **36**, 2308656.
37 W. M. Seong, K. Yoon, M. H. Lee, S.-K. Jung and K. Kang, *Nano Lett.*, 2018, **19**, 29–37.
38 Y. Yan, S. Weng, A. Fu, H. Zhang, J. Chen, Q. Zheng, B. Zhang, S. Zhou, H. Yan, C.-W. Wang, Y. Tang, H. Luo, B.-W. Mao, J. Zheng, X. Wang, Y. Qiao, Y. Yang and S.-G. Sun, *ACS Energy Lett.*, 2022, **7**, 2677–2684.
39 C. Zhang, X. Shen, X. Li, Q. Liu, Z. Liu, Y. Huang, Y. Gao, Z. Hu, J.-M. Chen, Y. Yang, J. Ma, S.-C. Haw, X. Wang, R. Yu, Z. Wang and L. Chen, *Chem. Mater.*, 2023, **35**, 6692–6701.
40 W. Ding, H. Ren, Z. Li, M. Shang, Y. Song, W. Zhao, L. Chang, T. Pang, S. Xu, H. Yi, L. Zhou, H. Lin, Q. Zhao and F. Pan, *Adv. Energy Mater.*, 2024, **14**, 2303926.